

UC San Diego

International Symposium on Stratified Flows

Title

The front condition for gravity currents propagating over rough boundaries

Permalink

<https://escholarship.org/uc/item/3s18t953>

Journal

International Symposium on Stratified Flows, 1(1)

Authors

Nokes, Roger
Cenedese, Claudia
Ball, Megan
[et al.](#)

Publication Date

2016-08-29

The Front Condition for Gravity Currents Propagating over Rough Boundaries

Roger Nokes¹, Claudia Cenedese², Megan Ball¹ and Tim Williams¹.

¹ Department of Civil and Natural Resources Engineering,
University of Canterbury
roger.nokes@canterbury.ac.nz

² Woods Hole Oceanographic Institution

Abstract

Gravity currents – fluid flows generated by horizontal density gradients – are ubiquitous in the environment. An area of increasing interest in this general field is the interaction of gravity currents with boundary roughness, where that roughness may be of the scale of the current itself. This paper describes an experimental study investigating the impact of varying boundary roughness densities on the flow structure and propagation speed of a gravity current. The gravity currents exhibit two primary flow regimes, a “flow through” regime where the current is enmeshed in the roughness elements, and an “overriding” regime where the current is forced to flow almost entirely over the roughness elements. As the flow transitions from the first to the second of these regimes through increasing roughness density there is the possibility that the Froude number of the current will actually increase.

1 Introduction

Gravity currents are a well-known, and well-researched, environmental fluid flow caused by horizontal density gradients. Simpson (1997) provides an excellent overview of the dynamics of these currents and their appearance in natural settings.

However much of the work to date has focused on currents propagating along smooth boundaries. Boundaries that incorporate roughness elements that are of a significant height compared to the current itself, while geophysically important, have received little attention. Nepf and her collaborators have made significant contributions to understanding fluid flow through canopies of various types. Zhang and Nepf (2011) explore the dynamics of a surface gravity current propagating through a suspended canopy comprising an array of circular cylinders using an experimental PIV system. The focus is to understand the exchange flow through the canopy. Nepf (2012) provides an overview of research in the area of flow through aquatic canopies.

This paper describes part of a larger investigation into the dynamics of currents encountering large roughness fields, focusing on the impact of the roughness on the flow structure and current propagation speed.

2 Methodology

2.1 Flume

Experiments were conducted in 6.2m long, 0.5m high and 0.25m wide flat-bottomed flume as illustrated in figure 1. A conventional lock exchange configuration was

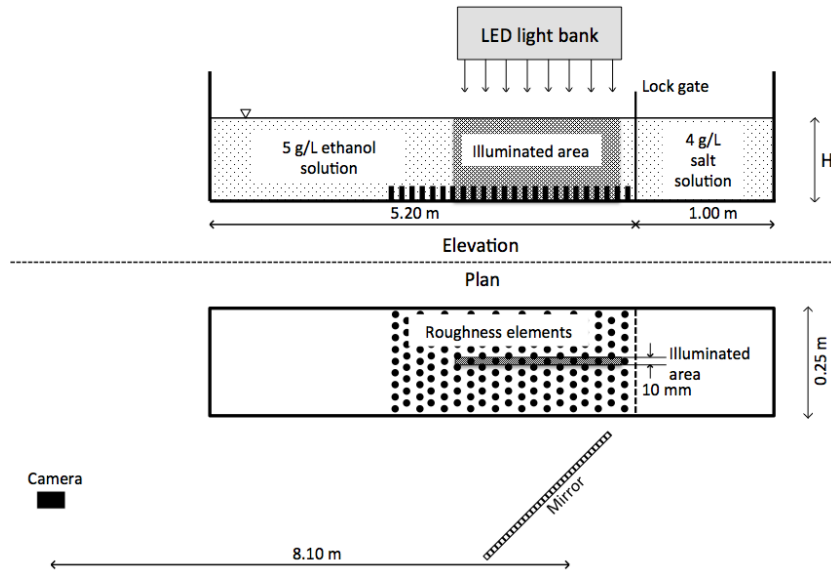


Figure 1: Elevation and plan view of the experimental setup.

employed to generate a dense gravity current. A stainless steel gate, sealed by plastic foam, was located 1 m from the right hand end of the flume. The bottom of the flume, for 3 m beyond the gate, was covered by a regular array of vertical, rigid, plastic cylinders – these cylinders being 2 cm in diameter and 5 cm high. The cylinders were screwed into an aluminum base plate and could be removed or added to produce varying roughness configurations.

The geometrical arrangement of the roughness elements could be characterized by three independent dimensionless parameters. These parameters are σ , the *plan density*, defined by

$$\sigma = \frac{A_P}{A_{TP}} \quad (1)$$

where A_P is the area of the base covered by the cylinders in plan and A_{TP} is the total area of the base in plan, μ , the *elevation density*, defined by

$$\mu = \frac{A_E}{A_{TE}} \quad (2)$$

where A_E is the area of the field covered by the cylinders in elevation as seen by the advancing current and A_{TE} is the total area of the field in elevation (measured to the top of the cylinders), and α , the *aspect ratio*, defined by

$$\alpha = \frac{h}{d} \quad (3)$$

where h is the height of the cylinders, d is their diameter.

For the roughness configurations utilized in this study (see figure 2) two of these parameters, α and μ , were fixed at values of 2.5 and 0.64 respectively, while the third parameter, σ , took three different values, 0.045, 0.09 and 0.18.

2.2 Initial conditions

The fluid behind the lock initially comprised a 4 g/l salt solution while that in the principal part of the flume was an ethanol solution selected to match the refractive

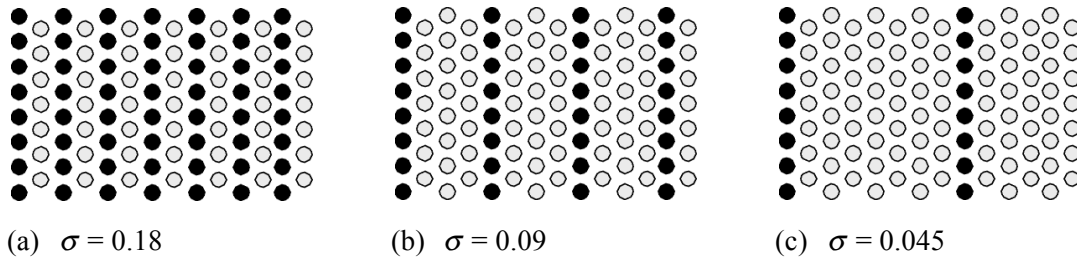


Figure 2: Plan view of the three experimental roughness configurations. Dark circles indicate occupied cylinder locations, and gray circles unoccupied cylinder locations. The gravity current propagates from left to right.

index of the salt water. The density difference between the two fluids, measured with an Anton Parr DMA5000 density meter, was approximately 0.5% for all experiments.

The depth of the fluid in the flume, H , relative to the roughness height provided a further dimensionless parameter associated with the flow's initial conditions. This *depth ratio*, defined as

$$\lambda = \frac{h}{H} \quad (4)$$

took values of 0.14, 0.19, 0.25 and 0.33 for each value of σ - corresponding to water depths of 350mm, 270mm, 200mm and 150mm respectively.

2.3 Velocity field measurement

For all experiments the flow was recorded using a particle tracking velocimetry (PTV) system. A 1.5m long white LED lightsheet generator, centred 1m downstream of the gate, produced an approximately 1cm wide light sheet along the centerline of the flume. Prior to the commencement of each experiment both fluids were seeded with 250-300 μ m pliolite particles and, once the gate was removed, the motion of these particles was captured with a JAI BB141GE video camera with zoom lens operating at 30.13Hz. The 1392x1040 pixel images were transferred directly to a fast hard drive on a PC during capture. The camera viewed the flow through an angled mirror in order to decrease the impact of parallax.

At the conclusion of an experiment the recorded images were analysed using the *Streams* software, (Nokes 2016). The final output from this analysis process was a non-dimensional 2D velocity field translated into the frame of reference of the gravity current front. The dimensionless variables used were

$$x' = \frac{x}{H}, \quad y' = \frac{y}{H} \quad (5)$$

and

$$u' = \frac{u}{U_f}, \quad v' = \frac{v}{U_f} \quad (6)$$

where x and y are the horizontal and vertical coordinates respectively with the origin of x' selected to be the location of the stagnation point at the nose of the current and

the origin of y' the flume bed. The two velocity components, u and v , were non-dimensionalised using the front speed, U_f .

The front velocity of a gravity current is relatively easy to determine if the current fluid is readily identifiable (for example if it is dyed) or the density field associated with the current is recorded. However obtaining the front speed from the velocity is more challenging. A number of different methods were implemented and the estimates obtained from these methods were averaged to determine the front speed. The spread of these estimates was used as an estimate of the error in the front speed and its non-dimensional equivalent, the Froude number, Fr , defined to be

$$Fr = \frac{U_f}{\sqrt{g'H}} \quad (7)$$

where g' is the reduced gravity given by

$$g' = g \left(\frac{\rho_s - \rho_e}{\rho_e} \right) \quad (8)$$

and g is the acceleration due to gravity, and ρ_s and ρ_e are the initial densities of the salt and ethanol solutions respectively.

2.4 Data quality and repeatability

It is acknowledged that there are intrinsic problems in obtaining robust time-averaged velocity fields using data recorded by a camera fixed in the laboratory frame of reference. There are two primary reasons for this. Firstly, the recording period is insufficient to be able to compute accurate Reynolds averages. Secondly it must be assumed that the current is in a quasi-steady flow regime such that the current front propagates at a constant speed and that the following internal flow is statistically stationary for the duration of the experiment. The impact of the first of these issues can be clearly seen in the lack of smoothness exhibited by the mean horizontal velocity field displayed in Figure 3.

To obtain some quantitative sense of the reliability of the velocity field data four repeat experiments were undertaken with $\lambda = 0.25$ and $\sigma = 0.18$. Figure 4 graphs the vertical profile of the time-averaged horizontal velocity at $x' = -1$. Despite the limitations due to the truncated time-averaging the repeatability of the experiments appears to be acceptable.

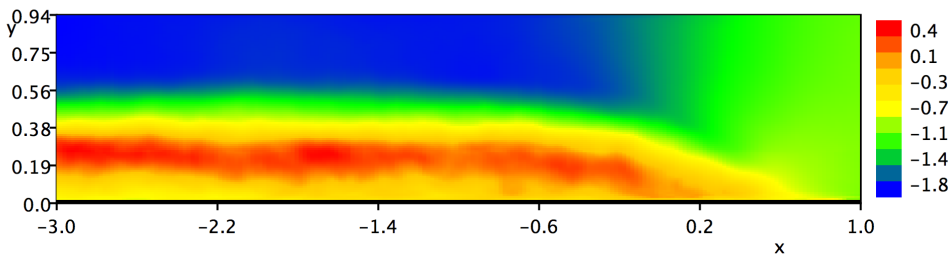


Figure 3: Time-averaged, steady state, non-dimensional horizontal velocity field for $\sigma = 0.04$ and $\lambda = 0.25$. Both x and y are dimensionless in this figure.

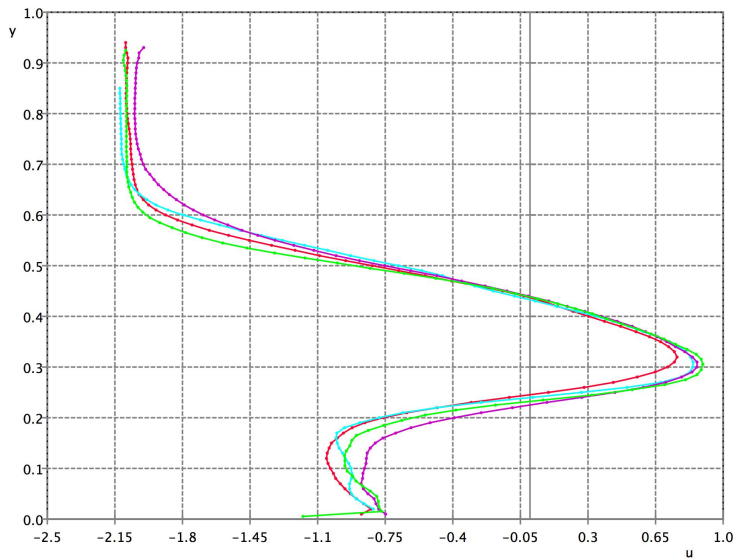


Figure 4. Vertical profiles of time-averaged horizontal velocity at $x' = -1$ for four repeat experiments with $\sigma = 0.04$ and $\lambda = 0.25$. Both u and y are dimensionless in this figure.

3 Results

3.1 Flow Regimes

In order to understand the flow behaviour it is valuable to consider the two extreme cases – $\sigma = 0$ and $\sigma = 1$. In the first case the bed is smooth and the current structure and Fr will match that of a standard lock exchange gravity current in the constant velocity regime. In the second case the roughness covers the entire boundary and once again the current will correspond to that over a smooth bed, with the slight difference that the initial fluid depth will be h less than that for the $\sigma = 0$ case.

It must be recognized that a limit of $\sigma = 1$ is not possible for all roughness layouts. In fact μ is the maximum value that σ can take. Thus, in general, and specifically for our configuration, the upper limit for σ is not 1.

For our experiments three fundamental flow regimes were observed as the value of σ changed. These are illustrated by the schematics in figure 5 which correspond to the flows for $\lambda = 0.25$. For the largest value of σ the obstruction presented to the current by the high concentration of roughness elements forced the current to predominantly flow above the elements despite the fact that the fluid within the elements was less dense than that above. The unstable buoyant exchange between the current fluid and that beneath is discussed in Cenedese, Nokes and Hyatt (2016). As σ decreases the current progressively shifts downwards such that ultimately the bulk of the current lies within the roughness field. For the smallest value of σ the current resembles a typical smooth bed current that occasionally encounters a porous wall that it must negotiate. The resulting flow structure for this smallest value of σ is clearly illustrated in figure 7 where the mean vertical velocity field in the laboratory frame of reference is plotted. While this flow is not steady the strong upflows and downflows caused by the individual ranks of cylinders is clear.

The cartoons in figure 5 illustrate two other key features of the flow that change with σ . The first is the location of the current front or nose. For small values of σ the nose is located just above the flume bed as seen in both figures 3 and 5. For relatively high values of σ the nose lies above the roughness elements as if the top of the elements was a mixed slip/no-slip boundary. Between these limits there is a mixed regime where two noses can form, one above the roughness elements and a second within the elements. In the case illustrated in figure 5b the nose within the elements leads that above. The second feature is the existence of turbulent wakes behind the cylinders. As σ decreases these wakes decrease in their spatial influence and their associated drag has a reducing impact on the front speed.

These flow regimes are also illustrated in the dependence on the depth ratio. Figure 6 provides schematics of the flow structure for a fixed roughness configuration but varying current height. For small λ the current resembles the “flow through” regime illustrated in figure 5c. As λ increases the flow transitions to the “overriding” regime.

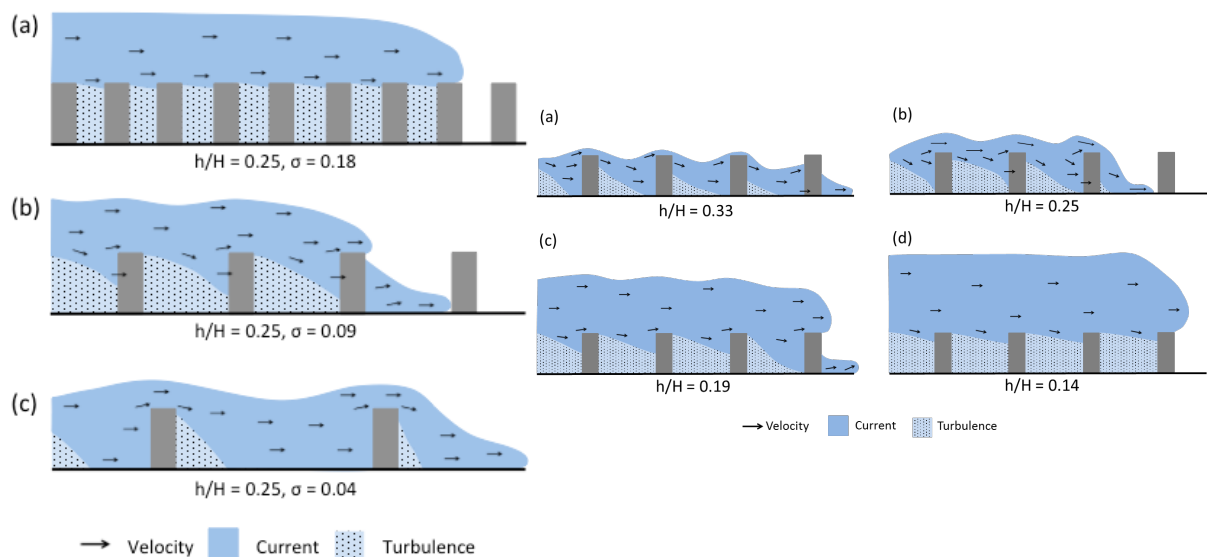


Figure 5. Schematics of the flow structure for fixed $\lambda = 0.25$ and variable σ (a) $\sigma = 0.18$ (b) $\sigma = 0.09$ (c) $\sigma = 0.04$.

Figure 6. Schematics of the flow structure of for fixed $\sigma = 0.09$ and variable λ (a) $\lambda = 0.33$, (b) $\lambda = 0.25$, (c) $\lambda = 0.19$ (d) $\lambda = 0.14$.

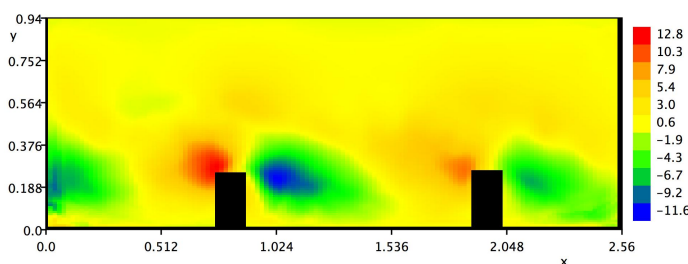


Figure 7. Time-averaged vertical velocity field in the laboratory frame of reference for $\sigma = 0.04$ and $\lambda = 0.25$. Both x and y are dimensionless in this figure. The apparently weaker motions to the right of the figure are due to the fact that the current is present at this location for only some of the averaging period.

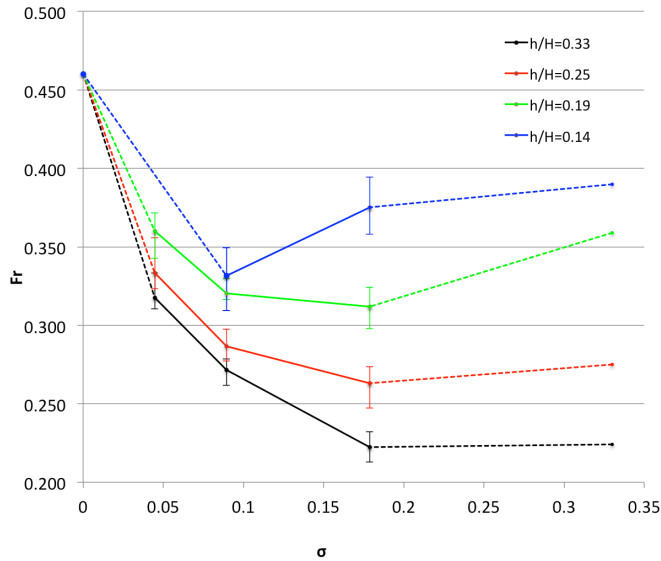


Figure 8. Fr dependence on σ , including data from Cenedese et al (2016) for $\sigma = 0$ and $\sigma = 0.33$. The solid lines are linear interpolations between the data from this study while the dashed lines interpolate between the data from this study and that of Cenedese et al (2016).

3.2 Front Condition

Of particular interest is the dependence of the Fr on the plan density, σ , and the depth ratio, λ . The results from these experiments, together with additional results from Cenedese et al (2016) are plotted in figure 8. The smooth bed Fr for fully turbulent high Re , currents, taken from the study by Cenedese et al (2016), is 0.46. To enable a point of comparison for a higher value of σ the results from Cenedese et al (2016) for $\sigma = 0.33$ are also plotted. These results need to be treated with caution as the value of μ does not match that for the current experiments. The configuration to which these data correspond includes cylinders placed at every location in figure 2a.

The data presented in figure 8 illustrate two key trends. Firstly, for fixed σ , Fr decreases with increasing depth ratio. The reason for this is clear as shallower currents see relatively larger obstacles in their path and therefore experience relatively greater drag. Secondly there is strong evidence that Fr reaches a minimum for some value of σ , and the location of this minimum is likely to vary with λ . While the proposition that increasing roughness leads to increasing current speed sounds counter-intuitive an understanding of the flow regimes described in section 3.1 provides sound evidence for this phenomenon.

The curves in figure 8 suggest that the value of σ , at which the minimum in Fr occurs, increases with increasing depth ratio. This is consistent with the previous observation that currents with smaller depth ratios transition to the overriding flow regime earlier than those with larger depth ratios and hence the apparent reduction in drag happens earlier for these deeper currents.

4 Conclusions

Experiments that explore the impact of a field of significant roughness elements on a bottom boundary gravity current have been described. The results from a PTV

measurement system indicate that the current will adopt a flow regime lying somewhere between two extremes – an “overriding” regime where the current effectively propagates atop the roughness elements and a “flow through” regime where the current lies within the roughness elements. As the density of the roughness elements increases currents transition from the “flow through” regime to the “overriding” regime with the result that the Fr of the currents can actually increase.

References

Cenedese, C., Nokes, R. and Hyatt J. (2016) Dynamics of lock-release gravity current over a sparse and dense rough bottom, VIIIth ISSF, San Diego, 2016.

Nepf, H. (2012) Flow and transport in regions with aquatic vegetation. *Annual Review of Fluid Mechanics*, 44:123-142.

Nokes, R. (2016) Streams 2.05 - System Theory and Design, *University of Canterbury*

Simpson, J. E. (1997) Gravity currents in the environment and the laboratory, 2nd Ed., *Cambridge University Press*, Cambridge.

Zhang, X. and Nepf H. (2011) Exchange flow between open water and floating vegetation. *Environmental Fluid Mechanics*, 11:531:546.